

## 7.1. Low-Coherence Interferometry (LCI)

Let us consider a typical Michelson interferometer, where a broadband source is used for illumination (Fig. 1a).

The light is split by the beam splitter (BS) and directed toward two mirrors, M1 and M2, which reflect the field back. Mirror M2 has an adjustable position, such that the phase delay between the two fields can be tuned. Finally, the two beams are recombined at the detector, via the BS (note that power is lost at each pass through the BS).

Examples of low-coherence sources include light emitting diodes (LEDs) superluminescent diodes (SLD), Ti:Saph lasers, and even white light lamps. Of course, the term “low-coherence” is quite vague, especially since even the most stabilized lasers are of finite coherence length. Generally, by low-coherence we understand a field that has a coherence length of the order of tens of microns (wavelengths) or less. We found previously (Section 3.3.) that the *coherence length* of a field with central wavelength  $\lambda_0$  and bandwidth  $\Delta\lambda$  is of the order of  $\tau_c = \lambda_0^2 / \Delta\lambda$ . A qualitative comparison between the optical spectrum of a broadband source and that of a laser is shown in Fig. 1b.

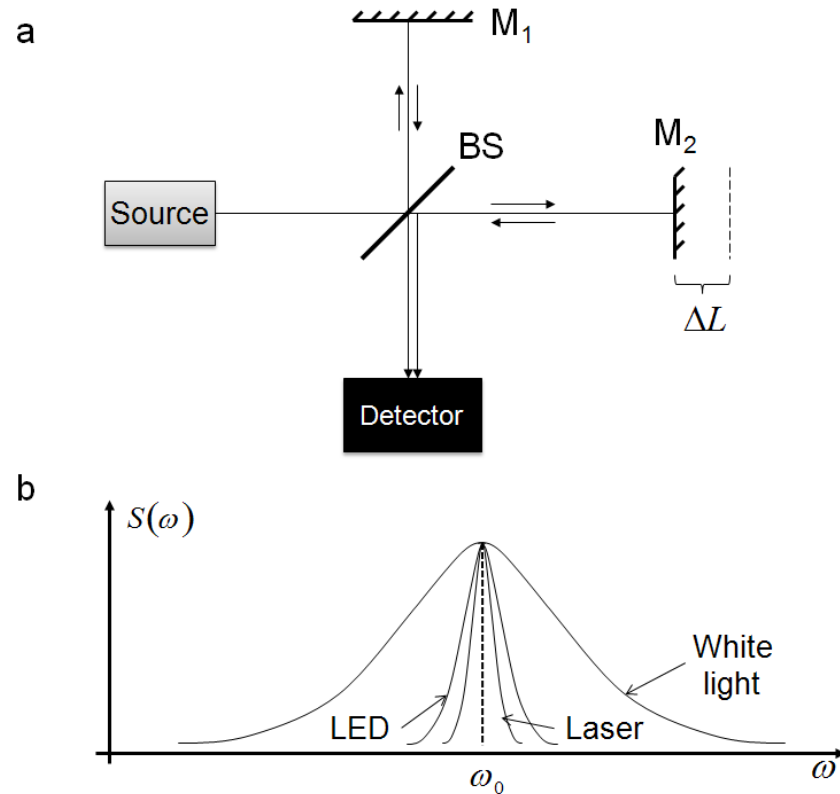


Figure 1. a) LCI using a Michelson interferometer. Mirror  $M_2$  adjusts the path-length delay between the two arms. b) Illustration of optical spectrum for various sources.

Let us now calculate the LCI signal in this Michelson interferometer. The total *instantaneous* field at the detector is the sum of the two fields,

$$U(t) = U_1(t) + U_2(t + \tau) \quad 1$$

where  $\tau$  is the delay introduced by the mobile mirror ( $M_2$ ),  $\tau = 2\Delta L/c$  (the factor of 2 stands for the double pass through the interferometer arm). The intensity at the detector is the *modulus-squared average* of the field,

$$\begin{aligned} I(\tau) &= \langle |U(t)|^2 \rangle \\ &= I_1 + I_2 + \langle U_1(t) \cdot U_2^*(t + \tau) \rangle + \langle U_1^*(t) \cdot U_2(t + \tau) \rangle \\ &= I_1 + I_2 + 2\text{Re}[\Gamma_{12}(\tau)], \end{aligned} \quad 2$$

where the angular brackets denote temporal averaging.

In Eq. 2 we recognize the temporal cross-correlation function  $\Gamma_{12}$ , defined as (see Section 3.3.)

$$\begin{aligned} \Gamma_{12}(\tau) &= \langle U_1(t) \cdot U_2^*(t + \tau) \rangle \\ &\propto \int U_1(t) \cdot U_2^*(t + \tau) dt \end{aligned} \quad 3$$

From Eq. 3, we see that the cross-correlation function can be measured experimentally by simply scanning the position of mirror  $M_2$ . Using the (generalized) Wiener-Kintchin theorem,  $\Gamma_{12}$  can be expressed as a Fourier transform

$$\Gamma_{12}(\tau) = \int W_{12}(\omega) \cdot e^{-i\omega\tau} d\omega. \quad 4$$

In Eq. 4,  $w_{12}$  is the cross-spectral density [2], defined as

$$W_{12}(\omega) = U_1(\omega) \cdot U_2^*(\omega) \quad 5$$

Note that  $w_{12}$  at each frequency  $\omega$  is obtained via measurements that are *time-averaged* over time scales of the order of  $1/\omega$ . Thus,  $W_{12}$  is inherently an average quantity.

For simplicity, we assume that the fields on the two arms are identical, i.e. the beam splitter is 50/50. We will study later the case of dispersion on one arm and the effects of the specimen itself. For now, if  $U_1(\omega) = U_2(\omega)$ ,  $W_{12}(\omega)$  reduces to the spectrum of light,  $S$ , and  $\Gamma_{12}$  reduces to the autocorrelation function,  $\Gamma$ ,

$$\Gamma(\tau) = \int S(\omega) \cdot e^{-i\omega\tau} d\omega.$$

6

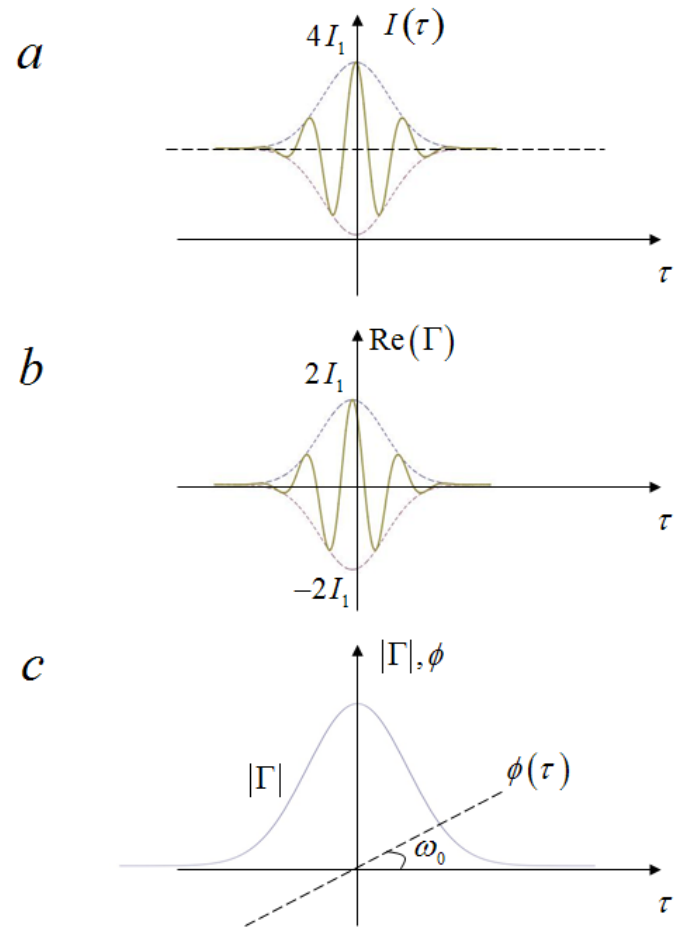


Figure 2. Low coherence interferometry with a perfectly balanced interferometer.

5

The intensity measured by the detector has the form shown in Fig. 2a. Subtracting the signal at large  $\tau$  (the DC component), which equals  $2I_1$  for perfectly balanced interferometers, the real part of  $\Gamma$  is obtained as shown in Fig. 2b. Therefore, as discussed in Appendix A, we can calculate the complex analytic signal associated with this measured signal. Using the Hilbert transformation, the imaginary part of  $\Gamma$  can be obtained as,

$$\text{Im}[\Gamma(\tau)] = -\frac{1}{\pi} P \int \frac{\text{Re}[\Gamma(\tau')]}{\tau - \tau'} d\tau', \quad 7$$

where P indicates a principal value integral. Thus, the *complex analytic signal* associated with the measured signal,  $\text{Re}[\Gamma(\tau)]$ , is the autocorrelation function  $\Gamma$ , characterized by an amplitude and phase, as illustrated in (Fig. 2c).

For a spectrum centered at  $\omega_0$ ,  $S(\omega) = S'(\omega - \omega_0)$ , it can be easily shown (via the shift theorem, see Appendix B) that the autocorrelation function has the form

$$\begin{aligned} \Gamma(\tau) &= \int S'(\omega - \omega_0) \cdot e^{-i\omega\tau} d\omega \\ &= e^{i\omega_0\tau} \int S'(\omega) \cdot e^{-i\omega\tau} d\omega \\ &= |\Gamma(\tau)| \cdot e^{i\omega_0\tau} \end{aligned} \quad 8$$

Equation 8 establishes that the envelope of  $\Gamma$  equals the Fourier transform of the spectrum. If we assumed a symmetric spectrum, the envelope is a real function. Further, the phase (modulation) of  $\Gamma$  is linear with  $\tau$ ,  $\phi(\tau) = \omega_0 \tau$ , where the slope is given by the mean frequency,  $\omega_0$ ,  $\phi(\tau) = \omega_0 \tau$ .

This type of LCI measurement forms the basis for time-domain optical coherence tomography (Section 7.3.). The name “time-domain” indicates that the measurement is performed in time, via scanning the position of one of the mirrors. Alternative, frequency domain, measurements will be also discussed in Section. 7.4.

## 7.2. Dispersion effects

In practice, the fields on the two arms of the interferometer are rarely identical. While the amplitude of the two fields can be matched via attenuators, making the optical pathlength identical is more difficult. Here, we will study the effect of dispersion due to the two beams passing through different lengths of dispersion media, such as glass. This is always the case when using a thick beam splitter in the Michelson interferometer (Fig. 3).

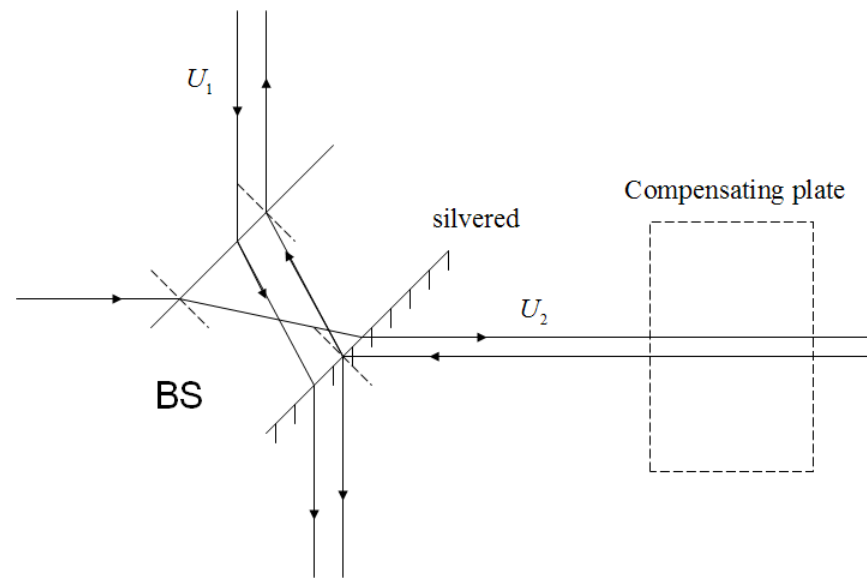


Figure 3. Transmission of the two beams through a thick beam splitter.



Typically, the beam splitter is made of a piece of glass half-silvered on one side.

It can be seen in Fig. 3 that field  $u_1$  passes through the glass 3 times, while field  $u_2$  passes through only once.

Therefore the phase difference between  $u_1$  and  $u_2$  has the frequency dependence

$$\begin{aligned}\phi(\omega) &= 2k(\omega)L \\ &= 2n(\omega)k_0L,\end{aligned}\tag{9}$$

where  $L$  is the thickness of the beam splitter,  $k_0$  the vacuum wavenumber, and  $n$  the frequency-dependent refractive index. This *spectral phase* can be expanded in Taylor series around the central frequency,

$$\phi(\omega) = \phi(\omega_0) + 2L \left. \frac{dk(\omega)}{d\omega} \right|_{\omega=\omega_0} (\omega - \omega_0) + L \cdot \left. \frac{d^2k}{d\omega^2} \right|_{\omega=\omega_0} (\omega - \omega_0)^2 + \dots\tag{10}$$

In Eq. 10, the individual terms of the Taylor expansion correspond to the following quantities:

phase shift of mean frequency,

$$\phi(\omega_0) = \frac{2\omega_0}{c} \cdot L,\tag{11}$$

group velocity,

$$v_g = \left. \frac{d\omega}{dk} \right|_{\omega=\omega_0}, \quad 12$$

group velocity dispersion (GVD)

$$\begin{aligned} \beta_2 &= \left. \frac{d^2k}{d\omega^2} \right|_{\omega=\omega_0} \\ &= \frac{\partial}{\partial \omega} \left( \frac{1}{v_g} \right) \cdot \end{aligned} \quad 13$$

GVD has units of  $s^2/m = s/Hz \cdot m$  and defines how a light pulse spreads in the material due to dispersion effects (delay per unit frequency bandwidth, per unit length of propagation). Note that GVD is sometimes defined as a derivative with respect to wavelength.

We can now express the cross-spectral density as

$$\begin{aligned}
W_{12}(\omega) &= U_1(\omega) \cdot U_1^*(\omega) \cdot e^{i\phi(\omega)} \\
&= S(\omega) \cdot e^{i\phi(\omega)} \\
&= S'(\omega - \omega_0) \cdot e^{i\phi(\omega_0)} \cdot e^{\frac{i2L}{v_g}(\omega - \omega_0)} \cdot e^{iL\beta_2(\omega - \omega_0)^2}
\end{aligned} \tag{14}$$

In Eq. 14 we assume that the two fields are of equal amplitude, and differ only through the phase shift due to the unbalanced dispersion, like, for example, due to the thick beam splitter shown in Fig. 3. The temporal cross-correlation function is obtained by taking the Fourier transform of Eq. 14. Let us consider first the case of negligible GVD, i.e.  $\beta_2 = 0$ ,

$$\begin{aligned}
\Gamma_{12}(\tau) &= e^{i\phi(\omega_0)} \int S'(\omega - \omega_0) \cdot e^{\frac{i2L}{v_g}(\omega - \omega_0)} \cdot e^{-i\omega\tau} d\omega \\
&= e^{i\omega_0\tau} \cdot e^{i\phi(\omega_0)} \int S'(\omega - \omega_0) \cdot e^{-i(\omega - \omega_0)\left(\tau - \frac{2L}{v_g}\right)} d(\omega - \omega_0)
\end{aligned} \tag{15}$$

Note that we can denote  $\omega - \omega_0$  as a new variable, to make it evident that the integral in Eq. 15 amounts to the shifted autocorrelation envelope,

$$\Gamma_{12}(\tau) = \left| \Gamma \left( \tau - \frac{2L}{v_g} \right) \right| \cdot e^{i(\omega_0 \tau + \phi(\omega))} \quad 16$$

Equation 16 establishes that, in the absence of GVD, there is no shape change in either the amplitude or the phase of the original correlation function. The phase shift,  $\phi(\omega_0)$ , is due to the zeroth order (*phase velocity*) term in the expansion of Eq. 10, while the envelope shift, or *group delay*, is caused by the first (*group velocity*) term (Fig. 4).

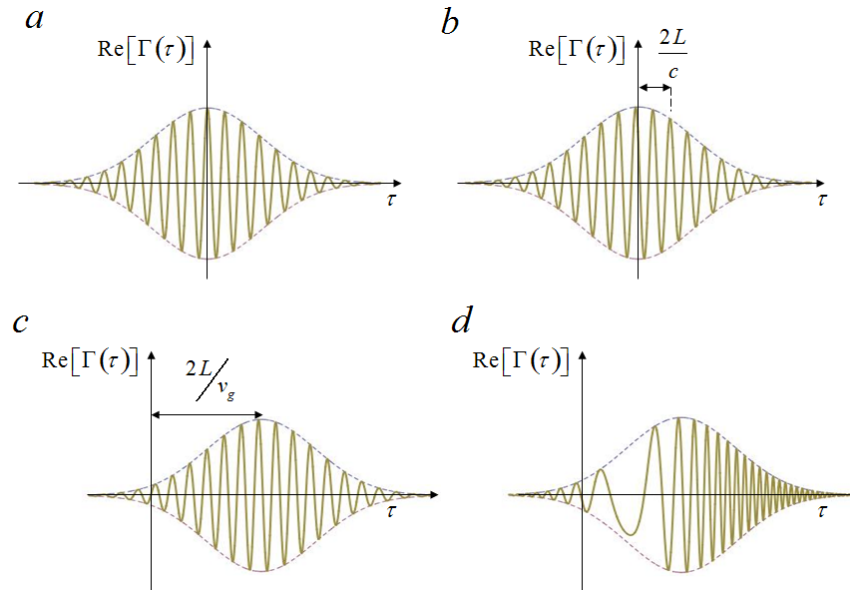


Figure 4. a) Autocorrelation function for a perfectly balanced detector. b) Phase delay (zeroth order) effects. c) Group delay (first order) effects. d) GVD (second order) effects.

Note that the envelope shift,  $\tau_0 = 2L/v_g$ , can be conveniently compensated by adjusting the position of mobile mirror of the interferometer. We conclude that if the beam splitter material has no GVD, the interferometer operates as if it is perfectly balanced.

Let us now investigate separately the effect of the GVD itself. The cross-correlation has the form

$$\Gamma_{12}(\tau) = \int S'(\omega - \omega_0) \cdot e^{iL\beta_2(\omega - \omega_0)^2} \cdot e^{-i\omega\tau} d\omega. \quad 17$$

Note that the Fourier transform in Eq. 17 yields a convolution between the Fourier transform of  $S'$  and that of  $e^{iL\beta_2\omega^2}$ , i.e.

$$\Gamma_{12}(\tau) = \Gamma(\tau) * e^{-i\frac{\tau^2}{4\beta_2 L}} / \sqrt{2\beta_2 L} \quad 18$$

Equation 18 establishes that the cross-correlation function  $\Gamma_{12}$  is broader than  $\Gamma$  due to the convolution operation.

Roughly, convolving two functions gives a function that has the width equal to the sum of the two widths (for Gaussian functions, this relationship is exact). Thus, if  $\Gamma$  has a width of  $\tau_c$  (i.e. coherence time of the initial light), the resulting  $\Gamma_{12}$  has a width of the order of  $\tau_{12} = \tau_c + \sqrt{2\beta_2 L}$ . Somewhat misleadingly, it is said in this case that the

*coherence time* (or length) “increased”, or that dispersion changes the coherence of light. In fact, the autocorrelation function for each field of the interferometer is unchanged. It is only their cross-correlation that is sensitive to unbalanced dispersion. Perhaps a more accurate description is to say that, in the presence of dispersion, the cross-correlation time is larger than the autocorrelation (coherence) time.

This dispersion effect ultimately degrades the axial resolution of OCT images, as we will see in the next section. In practice, great effort is devoted towards compensating for any unbalanced dispersion in the interferometer. Since Michelson’s time, this effect was well known; compensating for a thick beam splitter was accomplished by adding an additional piece of the same glass in the interferometer, such that both fields undergo the same number (three) of passes through glass.

### 7.3. Time-domain optical coherence tomography

OCT is typically implemented in fiber optics, where one of the mirrors in the interferometer is replaced by a 3D specimen (Fig. 5). In this geometry, the depth-information is provided via the LCI principle discussed above and the x-y resolution by a 2D scanning system, typically comprised of galvo-mirrors. The transverse (x-y) resolution is straight-forward, as it given by the numerical aperture of the illumination. Below we discuss in more detail the depth resolution and its limitation.

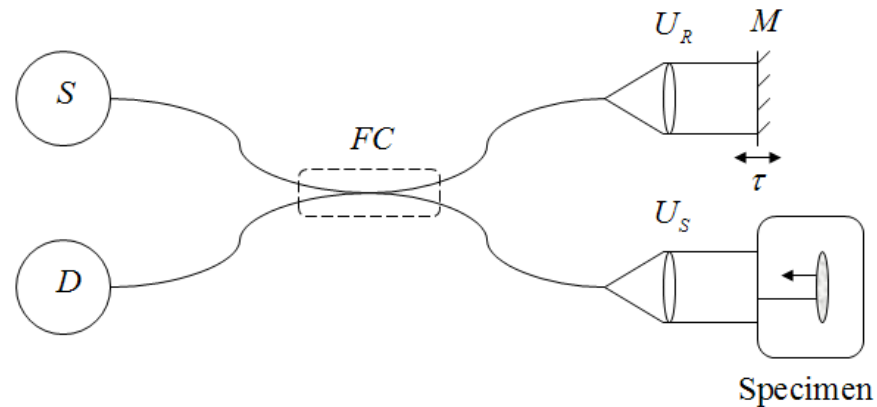


Figure 5. Fiber optic, time domain OCT.

At each point  $(x, y)$ , the OCT signal consists of the cross-correlation  $\Gamma_{12}$  between the reference field  $U_R$  and specimen field  $U_S$ , which can be expressed as the Fourier transform of the cross-spectral density

$$\begin{aligned} W_{12}(\omega) &= U_S(\omega) \cdot U_R^*(\omega) \\ &= S(\omega) \cdot \tilde{h}(\omega), \end{aligned} \quad 19$$

where  $S(\omega) = U_R(\omega) \cdot U_R^*(\omega)$  is the spectrum of the source and  $\tilde{h}(\omega)$  the *spectral modifier*, which is a complex function characterizing the spectral response of the specimen,

$$U_S(\omega) = U_R(\omega) \cdot \tilde{h}(\omega). \quad 20$$

The two fields are initially identical, i.e. the interferometer is *balanced*, and the specimen is modifying the incident field via  $\tilde{h}(\omega)$ . The resulting cross-correlation obtained by measurement is a convolution operation, as obtained by Fourier transforming Eq. 19.

$$\Gamma_{12}(\tau) = \Gamma(\tau) * h(\tau), \quad 21$$

where  $h$  is the time response function of the sample, the Fourier transform of  $\tilde{h}(\omega)$ ,



$$h(\tau) = \int \tilde{h}(\omega) \cdot e^{-i\omega\tau} d\omega.$$

22

### 7.3.1. Depth-resolution in OCT.

Note that the LCI configuration depicted in Fig. 1, i.e. having a mirror as object, is mathematically described by introducing a  $\delta$  response function,  $h(\tau) = \delta(\tau - \tau_0)$ . In this case the cross-correlation reduces to (from Eq. 21)

$$\Gamma_{12}(\tau) = \Gamma(\tau - \tau_0),$$

23

where  $\tau_0 = 2z/c$  represents the time delay due to the depth location  $z$  of the reflector (Fig. 6). In other words, by scanning the reference mirror, the position of the second mirror is measured experimentally with an accuracy given by the width of the cross-correlation function,  $\Gamma_{12}(\tau)$ .

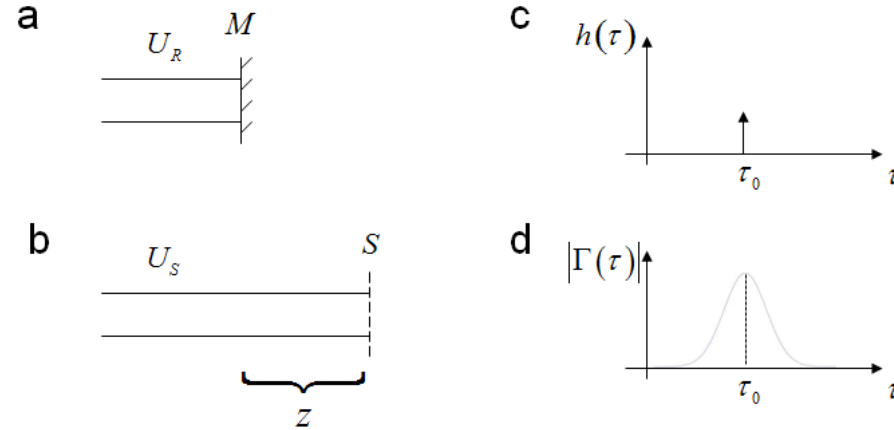


Figure 6. a) Response from a reflector at depth  $z$ : a) the reference arm; b) the sample arm; c) the ideal response function from the mirror in b; d) the measured response from the mirror in b.

OCT images are obtained by retaining the modulus of  $\Gamma_{12}$ , which is a complex function of the form

$\Gamma_{12}(\tau) = |\Gamma_{12}(\tau)| \cdot e^{i[\omega_0\tau + \phi(\tau)]}$ . Thus, the high frequency component (carrier),  $e^{i\omega_0\tau}$ , is filtered via demodulation (low-pass

filtering). Thus, the *impulse response* function of OCT is  $|\Gamma(\tau)|$ . As illustrated in Fig. 6b the width of the envelope of

$\Gamma$  establishes the ultimate resolution in locating the reflector's position. This resolution in time is nothing more than

the coherence time of the source,  $\tau_c$ , provided that the interferometer is balanced. In terms of depth, this resolution

limit is the *coherence length*,  $l_c = v\tau_c$ , with  $v$  the speed of light in the medium. This result establishes the well known

need for broadband sources in OCT, as  $\tau_c \propto \frac{1}{\Delta\omega}$ .

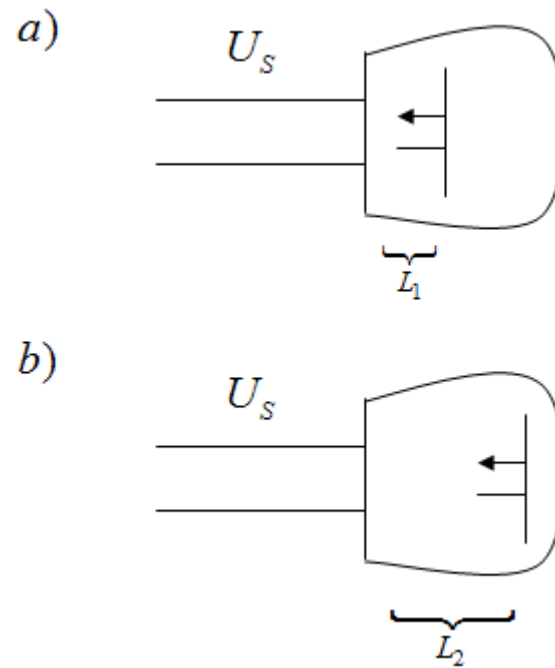


Figure 7. Depth-dependent resolution in OCT.

It is important to realize that the coherence length is the absolute best resolution that OCT can deliver. As mentioned in the previous section, the performance can be drastically reduced by dispersion effects due to an unbalanced interferometer. Further, note that the specimen itself does “unbalance” the interferometer. Consider a reflective surface buried in a medium characterized by dispersion (e.g. a tumor located at a certain depth in the

tissue), as illustrated in Fig. 7. Even when the attenuation due to depth propagation is negligible (weakly scattering, low-absorption medium), the spectral phase accumulated is different for the two depths (see Eq. 18),

$$\Gamma_{12}(\tau, L_{1,2}) = \Gamma(\tau) * e^{-i\frac{\tau^2}{4\beta_2 L_{1,2}}} / \sqrt{2\beta_2 L_{1,2}}, \quad 24$$

where  $\beta_2$  is the GVD of the medium above the reflector.

Therefore, the impulse response is broader from the reflector that is placed deeper ( $L_2 > L_1$ ) in the medium. This is to say that in OCT the axial resolution degrades with depth.

### 7.3.2. Contrast in OCT

Contrast in OCT is given by the difference in reflectivity between different structures, i.e. their refractive index contrast. OCT contrast in a transverse plane (x-y, or *en face*) also depends on depth. Figure 8 illustrates the change in SNR with depth. As can be seen, the scattering properties of the surrounding medium are affecting SNR in a depth-dependent manner. Thus, the backscattering ultimately limits the *contrast to noise ratio* in an x-y image.

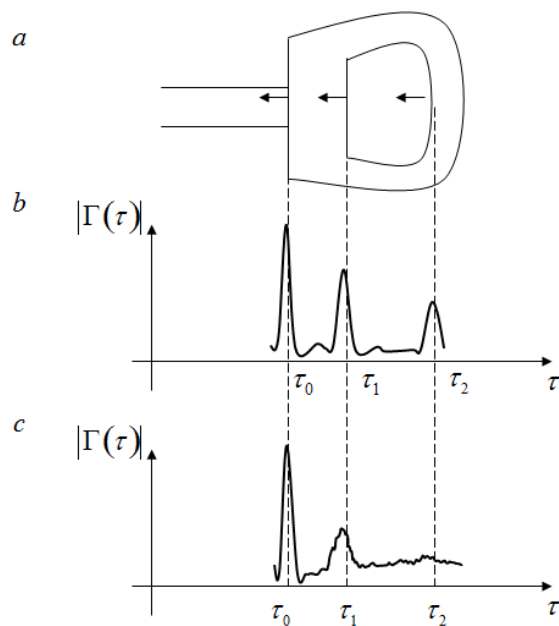


Figure 8. Signals from an object surrounded by scattering medium, illustrated in a). b) Depth-resolved signals for weakly scattering medium. c) Depth-resolved signals for strongly scattering medium.

The signal and noise can be defined at each depth, as

$$SNR(\tau) = \frac{|\Gamma_{12}(\tau)|}{\sigma_N(\tau)}, \quad 25$$

where  $\sigma_N(\tau)$  is the standard deviation of the noise around the time delay  $\tau$ . This noise component is due to mechanical vibrations, source noise, detection/electronic noise, but, most importantly, due to the scattering from the medium that surrounds the structure of interest.

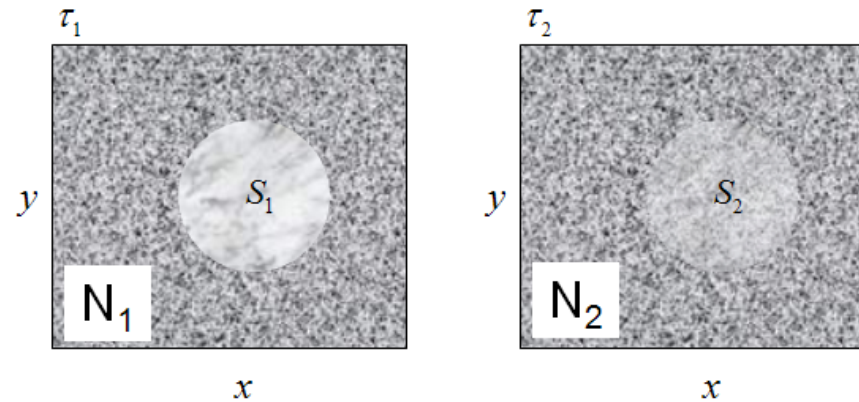


Figure 9. En-face images corresponding to the two time-delays shown in Fig. 8.

In an *en face* image, we can define the contrast to noise ratio as (Fig. 9)

$$CNR(\tau) = \frac{\left| |\Gamma_A(\tau)| - |\Gamma_B(\tau)| \right|}{\sigma_N(\tau)}, \quad 26$$

where A and B are two structures of interest.

#### 7.4. Fourier Domain and Swept Source OCT

The need for mechanical scanning in time domain OCT limits the acquisition rate and is a source of noise that ultimately affects the phase stability in the measurements (note that generally OCT is *not* a common path system). Fortunately, there is a faster method for measuring the cross-correlation function,  $\Gamma_{12}(\tau)$ . Thus, it is entirely equivalent to obtain  $\Gamma_{12}$  by measuring first the cross-spectral density,  $w_{12}(\omega)$ , and take its Fourier transform numerically, i.e. exploiting the generalized Wiener-Kintchin theorem,

$$\Gamma_{12}(\tau) = \int W_{12}(\omega) \cdot e^{-i\omega\tau} d\omega. \quad 27$$

In 1995, Fercher et al., from University of Vienna, applied this idea to obtain depth scans of a human eye [3]. They also pointed out that  $w_{12}(\omega)$  can be measured either by a spectroscopic measurement, where the colors are dispersed onto a detector array, or by *sweeping* the wavelength of the source and using a single (point) detector.

The principle of these frequency domain measurements is illustrated in Fig. 10.



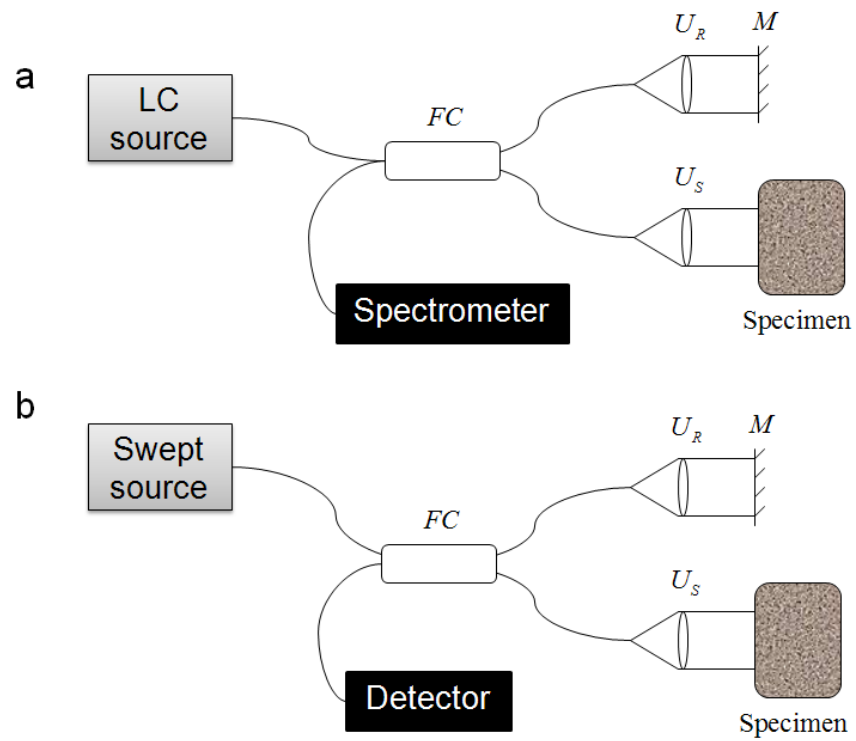


Figure 10. a) Fourier Domain OCT. b) Swept source OCT.

The total field at the spectrometer in Fourier domain OCT (Fig. 10a) is

$$U(\omega) = U_R(\omega) + U_S(\omega), \quad 28$$

Where  $U_R$  and  $U_S$  are the reference and specimen fields, respectively. As before, the frequency response of the object can be described by a complex function, the *spectral modifier*,  $\tilde{h}(\omega)$ , such that the field returned from the specimen can be written as

$$U_S(\omega) = U_R(\omega) \tilde{h}(\omega) e^{-i\omega s_0 / c}. \quad 29$$

In Eq. 29 the phase factor  $e^{-i\omega s_0 / c}$  indicates that the two arms of the interferometer are mismatched by a pathlength  $s_0$ , which is fixed. The intensity vs. frequency detected by the spectrometer results from combining Eqs. 28 and 29,

$$\begin{aligned} I(\omega) &= |U(\omega)|^2 \\ &= S(\omega) + S(\omega) |\tilde{h}(\omega)|^2 + 2S(\omega) |\tilde{h}(\omega)| \cos[\omega s_0 / c + \phi(\omega)]. \end{aligned} \quad 30$$

In Eq. 30,  $\phi(\omega)$  is the spectral phase associated with the object, i.e. the argument of the frequency modifier  $\tilde{h}(\omega)$ .

We can re-write Eq. 30 to better emphasize the DC and modulated terms,

$$I(\omega) = a(\omega) \{1 + b(\omega) \cdot \cos[\omega s_0 / c + \phi(\omega)]\}, \quad 31$$

where

$$a(\omega) = S(\omega) \left[ 1 + |\tilde{h}(\omega)|^2 \right],$$

$$b(\omega) = \frac{2|\tilde{h}(\omega)|}{1 + |\tilde{h}(\omega)|^2}.$$

32

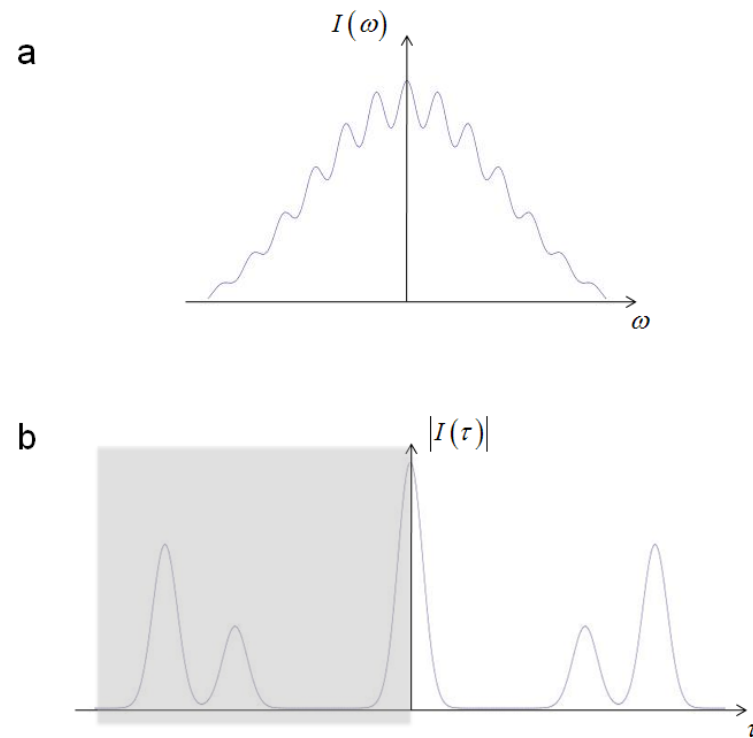


Figure 11. a) Typical row signal in Fourier domain OCT. b) Symmetric depth-resolved signal obtained by Fourier transforming the raw data.

A typical signal  $I(\omega)$  is illustrated in Fig. 11. Note that the modulation of the signal in Fig. 11 is quantified by the (real) function  $b(\omega)$  (Eq. 32b). This function can be easily shown to satisfy the relationships

$$\begin{aligned} 0 \leq b(\omega) \leq 1 \\ b(\omega) = 1 \text{ if } |\tilde{h}(\omega)| = 1 \end{aligned} \quad 33$$

Thus, not surprisingly, the highest contrast of modulation is obtained when the intensities of the two arms of the interferometer are equal,  $I_R(\omega) = I_S(\omega)$  and the specimen only affects the phase of the incident field.

In order to obtain the time domain response,  $I(\tau)$ , the measured signal  $I(\omega)$  is Fourier transformed numerically.

Since  $I(\omega)$  is a real signal, its Fourier transform is even (Fig. 11b). Let us consider for simplicity that the specimen has a “flat” frequency response in amplitude,  $|\tilde{h}(\omega)| = \text{const}$ , which is to say that the reflectivity of the object is not frequency dependent. In this case, the DC term, i.e. the Fourier transform of  $a(\omega)$ , is nothing more than the autocorrelation function  $\Gamma(\tau)$ . Further, let us consider that the object consists of a single reflective surface at depth  $z_0$ . In this case the modulated term in Eq. 31 has the form  $S(\omega) \cdot \cos[\omega s_0 / c - 2\omega z_0 / c]$ . The Fourier transform of this AC component has the form

$$I_{AC}(\tau) \propto \Gamma(\tau) * \left\{ \delta[(s_0 - 2z_0)/c] + \delta[(s_0 + 2z_0)/c] \right\} .34$$

Clearly, according to Eq. 34, the depth position of the object,  $z_0$ , can be experimentally retrieved from either side bands (delta functions), as shown in Fig. 11b. Like in time-domain OCT, the accuracy of this depth measurement is limited by the width of  $\Gamma(\tau)$ , which convolves the entire signal, i.e. the coherence length of the illuminating field.

The Fourier domain measurement is fully equivalent with its time domain counterpart.

Note that the pathlength mismatch,  $s_0$ , is fixed and sets the upper value for depth that can be accessed in the specimen,  $z_{\max} = s_0 / 4n$ , where  $n$  is the refractive index of the specimen. This can be easily understood by noting that the modulation of the  $I(\omega)$  signal must be at least twice the maximum frequency of interest, i.e.

$$s_0 \omega / c \geq 2s_{\max} \omega / c = 4nz_{\max} \omega / c .$$

The description above holds valid for swept-source OCT as well, the only difference being that the frequency components of  $I(\omega)$  are measured in succession rather than simultaneously. Recent developments in laser sources allow sweeping broad spectra at very high speeds, up to *100 kHz* [4].

In summary, Fourier domain OCT offers a fast alternative to acquiring depth-resolved signals. The detection via spectrometer makes the measurements *single shot*, such that the phase information across the measured signal  $I(\omega)$  is stable. This feature is the premise for using such a configuration in achieving point-scanning QPI. Below we describe the main developments associated with phase-sensitive imaging. Depending on whether or not the phase map associated with an object is retrieved quantitatively (in radians), we divide the discussion in qualitative (Section 7.5.) and quantitative methods (Section 7.6.).